

Effect of PFDTs/TiO₂ Coating on Microstructure and Wetting Behavior of Phosphogypsum

Yuanxia Li, Fangfang Zeng, Guang Yang, Yi Li, Shun Zhang, and Qibin Liu*

Cite This: *ACS Omega* 2024, 9, 39682–39695

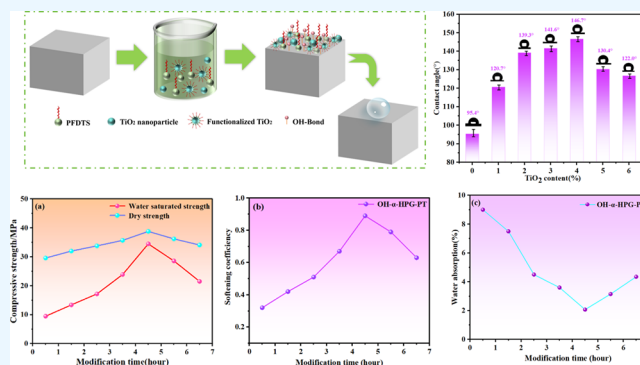
Read Online

ACCESS |

Metrics & More

Article Recommendations

ABSTRACT: Phosphogypsum (PG) constitutes a form of solid byproduct emanating from the manufacturing process of wet-process phosphoric acid. The fabrication of one metric ton of wet-process phosphoric acid entails the generation of approximately five tons of phosphogypsum, a highly prolific and economically viable waste stream. If we can effectively solve the problem of poor hydrophobicity of phosphogypsum, it is possible to replace cement and other traditional cementitious materials. In this way, we can not only improve the utilization rate of phosphogypsum but also obtain significant economic and environmental benefits. In the present investigation, hydrophobic surface coatings were synthesized and applied onto the surface of α -hemihydrate phosphogypsum (α -HPG) utilizing sol–gel processing and impregnation techniques. After hydroxylating α -HPG with alkaline solution (OH- α -HPG), titanium dioxide nanoparticles (TiO₂) hybridized with perfluorodecyltriethoxysilane (PFDTs) were grafted on its surface. The assessment of the hydrophobic properties of the coatings was conducted through water contact angle measurements, Fourier transform infrared (FTIR) spectroscopy, X-ray photoelectron spectroscopy (XPS), and scanning electron microscopy (SEM) analyses. The contact angle remained above 124.2° after strong acidic and alkaline immersion and 50 tape adhesion experiments with good chemical stability and durability, and the mechanism of surface hydrophobicity modification was discussed. The experimental outcomes demonstrated a notable increase in the hydroxyl group concentration on the α -HPG surface following hydroxylation, significantly enhancing the attachment rate of PFDTs and TiO₂ onto the HPG surface. PFDTs and TiO₂ can undergo chemical interaction with hydroxyl groups, facilitating their robust adsorption onto the surface of OH- α -HPG through chemisorption mechanisms. After bonding the OH- α -HPG surface with PFDTs and TiO₂ via hydrogen bonding, the otherwise hydrophilic α -HPG surface acquired excellent hydrophobicity (OH- α -HPG-PT, contact angle (CA) = 146.7°). The surface modification of α -HPG through hydroxylation and hydrophobicity enhancement significantly augmented the compatibility and interfacial interplay between α -HPG and PT. This research successfully enhanced the hydrophobic properties of α -HPG, profoundly showcasing its immense potential within the construction industry and the realm of comprehensive solid waste utilization.



1. INTRODUCTION

Phosphoric acid, an important industrial product, plays a vital role in both the chemical industry and agriculture. In the industrial wet-process production of phosphoric acid, phosphorus-based chemical enterprises generate phosphogypsum, a form of solid waste byproduct. The rapid proliferation of the phosphorus chemical industry is accompanied by statistics from participating companies indicating the generation of approximately 5 tons of phosphogypsum solid waste for every ton of phosphoric acid produced. Globally, phosphogypsum waste from phosphoric acid production in the phosphorus chemical industry exceeds 28.03 billion tons¹ China's phosphogypsum production is growing at a rate of 1.5 billion tons per year. The annual production of phosphogypsum in China continues to escalate at a rate of 150 million tons per annum, accounting for about 15% of the global total. The

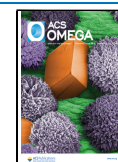
five provinces with the largest phosphogypsum production are Hubei, Yunnan, Guizhou, Sichuan, and Anhui.² The five provinces with the largest phosphogypsum production are Hubei, Yunnan, Guizhou, Sichuan and Anhui. It is predicted that the total amount of accumulated phosphogypsum will double in the future. Currently, the main methods of phosphogypsum disposal are landfills and underwater burials. However, the infiltration of impurities such as fluorine,

Received: May 22, 2024

Revised: August 16, 2024

Accepted: August 21, 2024

Published: September 6, 2024



phosphorus pentoxide and certain radioactive elements can pose a threat to phosphogypsum.³ The penetration of impurities such as The infiltration of impurities such as certain radioactive elements poses a threat to human survival, occupies land and causes environmental pollution. Therefore, the imperative challenge lies in devising strategies for harnessing phosphogypsum as a valuable resource, crucial for advancing the phosphorus chemical industry. Notably, phosphogypsum predominantly exhibits two distinct hues: gray-black and gray, white. The particles typically possess diameters ranging from 5 to 50 μm , with a crystallization content generally falling within 20 to 25%. The crystallization morphology predominantly encompasses needle-shaped, monodisperse plate-like, polycrystalline, and dense structures, among which plate-like crystals are the most prevalent. The main chemical composition of phosphogypsum is $\text{CaSO}_4 \cdot 2\text{H}_2\text{O}$ and SiO_2 . Furthermore, it contains various toxic and hazardous elements, including phosphorus (P), fluorine (F), arsenic (As), chromium (Cr), cadmium (Cd), trace metallic elements, and rare earth elements.⁴ Radionuclides, water-soluble phosphorus and fluorine in phosphogypsum tend to contaminate groundwater, leading to environmental pollution problems and restricting its use in construction materials.

The solubility of phosphogypsum in aqueous media is exceedingly low and undergoes a decrement with rising temperatures. Moreover, a more regular crystalline morphology and larger particle sizes of phosphogypsum correlate with lower impurity content.⁵ Through calcination and dehydration, the gelling activity of the original phosphogypsum can be stimulated, resulting in the formation of two types: β -type hemihydrate phosphogypsum (β -HPG) and α -type hemihydrate phosphogypsum (α -HPG).⁶ α -HPG has uniform grain size, with a small percentage of crystals being acicular and most being columnar. In contrast, β -HPG has an irregular grain size distribution with many small crystals. α -HPG exhibits superior crystallinity, minimal water demand, outstanding thermochemical stability, and high mechanical durability. It demonstrates remarkable performance in the fabrication of high-value products, making it suitable for utilization in cement and construction material production. Additionally, α -HPG can substitute a portion of calcium carbonate (CaCO_3) as a reinforcing filler in polymeric materials, thereby fostering the effective utilization of phosphogypsum resources. The primary objective of this research endeavor is to enhance the hydrophobic properties of α -HPG, which not only addresses environmental concerns but also curtails the production costs of composites while augmenting their water hydrophobicity.

The surface of phosphogypsum is hydrophilic and hydrophobic. Under high humidity or when exposed to moisture, it is prone to melt creep and alkalization, which negatively affects the mechanical properties. In addition, the use of phosphogypsum in pavement hardening is prone to the formation of caliche and subsequent expansion, resulting in pavement damage. As a porous air-hard cementitious material, phosphogypsum's poor moisture resistance and hydrophobicity limit its application in many areas.⁷ Therefore, it is important to prepare a hydrophobic phosphogypsum cementitious material.

Organic particles can effectively fill the capillary and microporous walls in the hardened structure of phosphogypsum, thus enhancing the hydrophobicity of phosphogypsum-based materials. Zhou et al.⁸ prepared unfired phosphogypsum ceramics with a dense hydrophobic layer by using

phosphogypsum as a substrate, grafting silane coupling agent on unfired phosphogypsum ceramics, and then coating them with unsaturated polyester resin. This research further delved into the influence of silane coupling agent on the macroscopic characteristics and microstructural features of unfired phosphogypsum ceramics. Deng et al.⁹ Examined the influence of organosilicon hydrophobic agents on the properties of phosphogypsum-based cementitious materials. The findings indicated that the incorporation of an optimal quantity of organosilicon hydrophobic agent resulted in a decrease in the porosity, pore diameter, and water absorption capacity of phosphogypsum, thereby enhancing its hydrophobic properties. At present, researchers at home and abroad mainly use organosilanes to improve the poor hydrophobicity of phosphogypsum. Although this method greatly improves the hydrophobicity of phosphogypsum samples without affecting the aesthetics of phosphogypsum products, there are still some drawbacks: first, the influence of organic hydrophobes primarily pertains to phosphogypsum featuring smaller pore sizes and lower porosity, whereas their effect on phosphogypsum characterized by larger pore sizes and higher porosity is negligible. Second, they contain large amounts of organic solvents, resulting in high costs and possible health and environmental hazards.

Therefore, the researchers found that the inorganic cementitious material, in addition to its high strength, low heat of hydration, high resistance to chemical erosion and environmental friendliness, exhibits the following characteristics.¹⁰ Whether it is a phosphogypsum sample with small pore size and low porosity or a phosphogypsum sample with large pore size and high porosity, it can significantly improve the hydrophobicity.¹¹ The surface modification of inorganic particles fortifies the interfacial interactions occurring between these particles and the polymer matrix.¹² Generally, organosilicon modifiers are employed to undergo chemical reactions with the hydroxyl groups present on the surface of inorganic nanoparticles (e.g., TiO_2 , SiO_2 , and alum, etc.) and graft-modify the surface of inorganic nanoparticles. The number of hydroxyl groups determines the grafting rate of the organic chains of the modifier that are eventually grafted onto the surface of the inorganic particles.¹³ The quantity of hydroxyl groups dictates the rate of grafting for the organic chains of the modifier, ultimately determining the extent of modification achieved on the surface of the inorganic particles. However, the limited availability of free hydroxyl groups on the surface of inorganic nanoparticles poses a challenge, the grafting rate of the modifier organic chains on the surface of inorganic nanoparticles is relatively low. Chen et al.¹⁴ Examined the influence of hydroxylation on the grafting of $(\text{CH}_3\text{O})_3\text{-Si-CH}_2\text{-CH}_2\text{-CH}_2\text{-NH}_2$ (APS) and the subsequent fabrication of CaSO_4 /polyvinyl chloride(PVC) composites. The findings indicate that the pretreatment of CaSO_4 particles with NaOH facilitates the generation of hydroxides, subsequently enhancing the grafting of APS onto the calcium sulfate surface and optimizing the interfacial adhesion between the calcium sulfate and PVC matrix. Goncalves et al.¹⁵ graphene oxide nanosheets were subjected to treatment with thionyl chloride and ethylene glycol, resulting in an augmentation of hydroxyl groups on their surface. This modification enhanced the grafting efficiency of poly(methyl methacrylate) (PMMA), leading to improved thermal stability of the resultant graphene oxide/PMMA nanocomposite films in comparison to graphene oxide fillers alone. Lu et al.¹⁶ conducted a study in which calcium

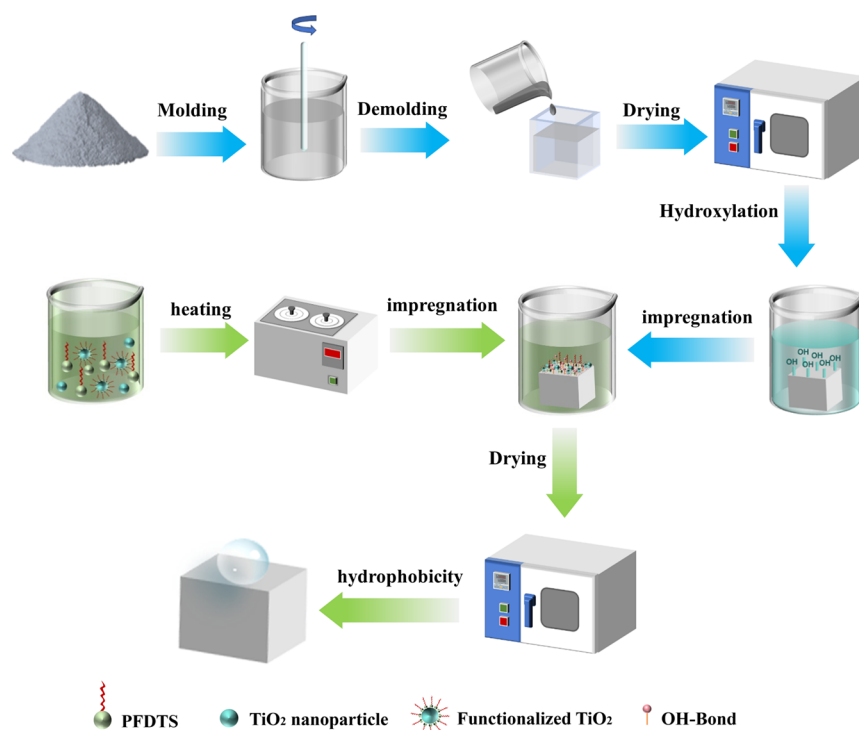


Figure 1. Schematic representation of surface hydrophobic coating prepared using PFDTs and TiO₂ nanoparticles.

sulfate whisker (CSW) was hydroxylated through treatment with NaOH, thereby increasing the density of hydroxyl groups on its surface. This was followed by modification with a polyether titanate coupling agent, which effectively bolstered the interfacial compatibility between CSW and PVC, ultimately resulting in a substantial improvement in the mechanical properties of the composite material. Phosphogypsum, characterized by a complex composition and a limited number of surface hydroxyl groups, inherently possesses a tendency for these groups to readily engage in hydrogen bonding with surrounding molecules, resulting in their deactivation. Consequently, prior to employing phosphogypsum as a filler in polymeric materials, it is imperative to undertake a pretreatment process aimed at producing α -HPG and subsequently hydroxylate its surface to augment the count of hydroxyl groups. This augmentation is crucial for enhancing the grafting efficiency of the organic chains of the modifier.

The number of hydroxyl groups on the α -HPG surface increases through a simple precipitation reaction with sodium hydroxide solution.¹⁷ Subsequently, PFDTs and TiO₂ reacted with the hydroxyl groups through hydrogen bonding, and thus adsorbed tightly on the OH- α -HPG surface by chemisorption. After bonding the α -HPG surface with PFDTs and TiO₂ via hydrogen bonding, the originally hydrophilic α -HPG surface acquired excellent hydrophobicity. The assessment of the phosphogypsum surface in terms of its hydrophobicity and microstructural properties was carried out through a multifaceted approach involving water contact angle measurements, Fourier transform infrared spectroscopy, X-ray photoelectron spectroscopy, and scanning electron microscopy. These analytical techniques were employed to comprehensively characterize and analyze the surface attributes of the phosphogypsum. In summary, the organosilicon modifier and inorganic nanoparticles filled with hydroxylated phosphogypsum capillaries complemented each other, which not only

reduced the porosity of phosphogypsum crystals, but also controlled their sizes, so that the phosphogypsum crystals were tightly connected to form a dense structure, thus improving their hydrophobicity and mechanical properties. Therefore, the composite of organic modifier and inorganic nanoparticles optimized the hydrophobicity and mechanical properties of phosphogypsum-based materials modified with organosilicon modifier or inorganic nanoparticles alone, and realized the effective and comprehensive utilization of phosphogypsum.¹⁸

2. MATERIAL AND EXPERIMENTAL DETAILS

2.1. Materials. α -HPG was purchased from Guizhou Phosphate Green Industry Co. PFDTs (molecular weight: 610.379, purity: 97%) was purchased from Shanghai Bide Pharmaceuticals Technology Co. TiO₂ nanoparticles (molecular weight: 79.87, purity: 98%, average particle size: 50 nm) was purchased from Aladdin Biochemistry Technology Co. NaOH (molecular weight: 40, purity: 96%) was purchased from Aladdin Biochemistry Technology Co. Anhydrous sodium sulfate (Na₂SO₄, analytically pure) was provided by Tianjin Jialin Chemical Reagent Co. Anhydrous ethanol (analytically pure) was purchased from Shanghai McLean Biochemical Technology Co.

2.2. Experimental Methods. **2.2.1. Surface Hydroxylation of α -HPG Samples.** The prepared α -HPG samples were 100 mm × 60 mm × 30 mm in size, with a water to pulp ratio (W/C) of 0.6. The molds were removed after 2 h of casting. After curing for 1 day in a standard maintenance box, the samples were dried in a (40 ± 5) °C blast drying oven for 24 h. The α -HPG samples were immersed in an acetone solution to remove impurities at a room temperature of approximately 25 °C. Following this, 5 g of sodium hydroxide and 0.3 g of sodium sulfate were incorporated into 30 g of deionized water. After 10 min of magnetic agitation, the α -HPG specimen was submerged in the alkaline solution for an additional 10 min.

After being subjected to drying in a convection oven maintained at a temperature of (40 ± 5) °C for a period of 24 h, the resulting hydroxylated α -type hemihydrate phosphogypsum sample (designated as OH- α -HPG) was obtained.

2.2.2. Surface Hydrophobic Modification of OH- α -HPG Samples. Figure 1 displays a scheme of hydrophobic coatings preparation on the surface of OH- α -HPG samples. The hydrophobic PFDTs/TiO₂ coating was based on Guo's report.^{19,20} Preparation and modification were carried out. Initially, 0.01% (v/v) of PFDTs was dissolved in 20 mL of ethanol as the solvent, followed by the addition of 0.8 g of TiO₂ nanoparticles to the resultant solution. Thereafter, the combined solution was subjected to heating and magnetic agitation within a water bath maintained at 45 °C for a duration of 15 min, resulting in the synthesis of a composite hydrophobic agent designated as PT. The OH- α -HPG sample was immersed in the PT solution for 24 h using the impregnation method. Subsequently, the sample underwent air-drying in a forced convection oven at a temperature of (40 ± 5) °C for a period of 24 h, resulting in the production of an α -type hemihydrate phosphogypsum sample (OH- α -HPG-PT) that was endowed with a surface hydrophobic coating.

2.3. Analytical Methods. To quantify the level of impurities, present in α -HPG, a standardized procedure for the chemical examination of gypsum and its derivatives, as outlined in the ASTM C471M-2017 standard (Indicator), was employed. The median particle diameter (d_{50}) was ascertained utilizing a laser diffraction-based particle sizing apparatus (Mastersizer 2000, Malvern Instruments, UK), while the particle size distribution span of the samples was derived in accordance with the formula presented in eq 1.²¹

$$\text{Span} = \frac{d_{90} - d_{10}}{d_{50}} \quad (1)$$

Where Span is the particle size distribution of the sample; d_{90} indicates that in the size distribution, 90% of the cumulative particle diameters are less than this value; d_{10} indicates that 10% of the cumulative particle diameters are less than this value; and d_{50} is the median diameter, i.e., 50% of the cumulative particle diameters are less than this value.

To ascertain the activation index, a precise quantity of 3.0 g of the α -HPG sample was weighed into a beaker, followed by the addition of 100 mL of deionized water. The resultant mixture was agitated at a constant speed of 300 rpm for a duration of 15 min at ambient temperature, and subsequently allowed to settle in a separatory funnel for 30 min. The activation index of the α -HPG sample was then mathematically derived in accordance with the formula outlined in eq 2.

$$H = \frac{m - m_0}{m} \times 100\% \quad (2)$$

Herein, H represents the activation index, %; m denotes the initial mass of the α -HPG sample, g; whereas m_0 signifies the weight of the α -HPG sample after attaining a constant weight, g.

The physical phase and particle size distribution characteristics of α -HPG were comprehensively examined employing a range of analytical techniques. Specifically, X-ray diffraction (XRD) analysis, conducted on an UltimaIV instrument (Rigaku, Japan), was utilized to elucidate the physical phase. Additionally, oxide composition was determined through X-ray fluorescence spectroscopy, utilizing an ARL Perform'X system

(Thermo Scientific, USA). Furthermore, the particle size distribution was precisely measured utilizing a laser particle sizer, namely the Mastersizer 2000 instrument, sourced from Malvern Panalytical (Nottingham, United Kingdom). To prepare the 100 mm × 60 mm × 30 mm α -HPG samples for hydrophobic treatment, an in situ polishing process was performed using sandpaper, aimed at eliminating impurities and achieving the desired surface roughness. Subsequently, the contact angles of the various sample surfaces were quantitatively assessed using an optical contact angle tester (model JC2000D1, manufactured by Shanghai Zhongchen Digital Technology Equipment Co., Ltd., Shanghai, China), employing 10 μ L of deionized water as the test liquid. Furthermore, the elemental composition of the surfaces of different α -HPG samples was analyzed through X-ray photoelectron spectroscopy (XPS), utilizing a K-Alpha Instruments system sourced from Thermo Scientific, located in Waltham, Massachusetts, Polymers MA, USA. During this analysis, all binding energies were calibrated against the C 1s peak of carbon, set at 284.8 eV, as a reference. The molecular structure and material chemical composition of the α -HPG samples were analyzed using a Fourier transform infrared spectrometer (Sigma 300, ZEISS, Oberkochen, Baden-Wurttemberg, Germany). The FTIR spectrometer operated within a spectral scanning range spanning from 400 to 4000 cm^{-1} .

The mass variation of the α -HPG sample as a function of temperature was quantitatively determined utilizing a TA Discovery TGA 550 Thermogravimetric Analyzer from TG USA, operated under precise instrumental temperature control conditions. The analysis was conducted in a nitrogen atmosphere, encompassing a specific temperature range from 30 to 650 °C, at a uniform heating rate of 10 °C/min. The surface grafting efficiency of the α -HPG was subsequently derived in accordance with the mathematical formulation outlined in eq 3.

$$\text{Grafting rate} = (W_A - W_B)/W_C \quad (3)$$

In this context, W_A represents the mass loss value observed for OH- α -HPG-PT upon heating to 600 °C, W_B denotes the mass loss value of either α -HPG or OH- α -HPG when subjected to heating up to 600 °C, and W_C signifies the residual weight fraction of OH- α -HPG-PT after being heated to 600 °C.

To evaluate the softening coefficient of OH- α -HPG-PT specimens, the samples underwent demolding and were promptly confined within a curing chamber, where they were subjected to standardized curing conditions for a period of 7 days. Subsequently, the cured OH- α -HPG-PT specimens were introduced into an oven maintained at 60 °C for drying until a constant mass was achieved. Following this, half of the dried specimens were immersed in water for a duration of 24 h, yielding water-saturated test specimens. The mechanical strength of both the soaked and the original dried samples was assessed in accordance with the GB/T9776-2008 standard. The softening coefficient of phosphogypsum is the fraction of the breaking strength of the sample in water to the ratio of absolute dryness.²² The softening coefficient of phosphogypsum represents the comparative measure of the fracture strength of a sample when it is fully saturated with water, relative to its fracture strength when in an absolutely dry state. This coefficient quantifies the degree of reduction in strength that occurs because of water absorption.

The softening coefficient (K_f) was calculated according to the following equation:¹⁸

$$K_f = \frac{R_f}{R_0} \quad (4)$$

Where K_f represents the softening coefficient, R_f denotes the breaking strength of the sample when immersed in saturated water, measured in megapascals (MPa), and R_0 signifies the breaking strength of the sample in its dry state, also expressed in megapascals (MPa).

3. RESULTS AND DISCUSSION

3.1. Compositional Analysis of α -HPG and β -HPG. The graphical representation of X-ray diffraction (XRD) analysis for HPG is depicted in Figure 2, and the main crystalline phases in

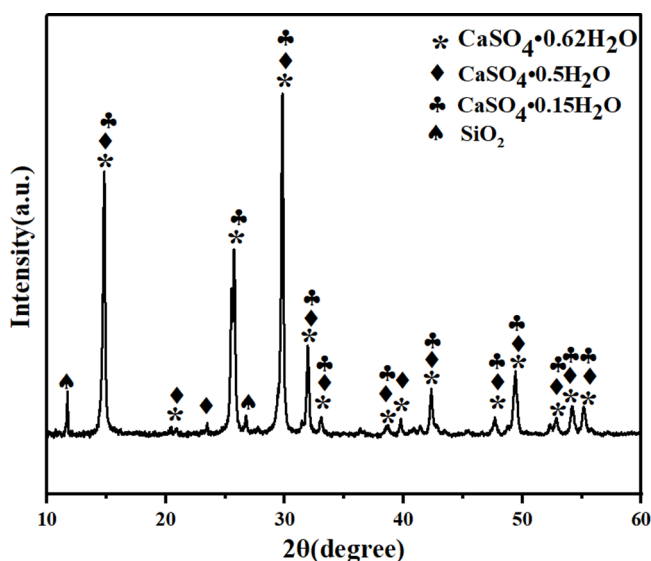


Figure 2. XRD spectrum of HPG.

HPG are $\text{CaSO}_4 \cdot 0.5\text{H}_2\text{O}$, $\text{CaSO}_4 \cdot 0.62\text{H}_2\text{O}$, $\text{CaSO}_4 \cdot 0.15\text{H}_2\text{O}$, and SiO_2 . The compositional breakdown of α -HPG and β -HPG is presented in Table 1, respectively. After calcination, PG can undergo a transformation into either α -hemihydrate phosphogypsum or β -hemihydrate phosphogypsum, both compositions consisting primarily of approximately 90 wt % (wt %) of $\text{CaSO}_4 \cdot 0.5\text{H}_2\text{O}$ (as determined from the proportions of SO_3 and calcium oxide) with minor inclusions of silica, phosphorus pentoxide, and alumina.²³ In α -HPG, the contents of SiO_2 , Al_2O_3 , Fe_2O_3 , K_2O , CeO and SrO were significantly lower, while the total contents of SO_3 and calcium oxide were significantly higher. Therefore, α -HPG has lower impurity content and better performance compared to β -HPG.²⁴

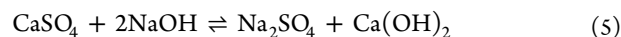
3.2. Preparation of α -HPG and β -HPG. α -HPG and β -HPG are two different phosphogypsum variants which were obtained as follows:

α -HPG is a powder cementitious material with α -type $\text{CaSO}_4 \cdot 0.5\text{H}_2\text{O}$ as the main phase, which is produced by

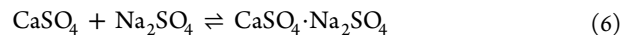
taking $\text{CaSO}_4 \cdot 2\text{H}_2\text{O}$ as the raw material in saturated water vapor medium or liquid aqueous solution under certain temperature, pressure or transcristallization agent conditions.²⁵ The common preparation methods are vaporization and compression method. Commonly used preparation methods are vaporization method,²⁶ hydrothermal method²⁷ atmospheric pressure salt solution method²⁸ and microwave irradiation method²⁹ and microwave irradiation. Compared with other methods, vaporization method is the most used method to prepare α -HPG crystals in the industry, which has the advantages of large output and easy control. Generally, the phosphogypsum is finely ground by grinding mill, and then passed into high-pressure water vapor, the pressure is controlled at 2–8 MPa, the steaming time is 1.5–10 h, and then dried, the drying temperature is 100–180 °C.

β -HPG is predominantly synthesized through the dry calcination process of phosphogypsum.³⁰ Prior to calcination, the phosphogypsum undergoes pretreatment stages including crushing, homogenization, and grinding. Subsequently, it is subjected to calcination at temperatures of 120, 150, and 200 °C to facilitate dehydration and promote the desired phase transformation reaction.³¹ The specific process is as follows: phosphogypsum, the specific process flow is phosphogypsum → flotation + cleaning → solid–liquid separation → cake drying → calcination → grinding → phosphogypsum powder finished product.

3.3. Hydroxylation of α -HPG. The reaction formula for hydroxylation of α -HPG using NaOH and Na_2SO_4 is as follows:³²



Upon dissolution of NaOH in water, dissociation occurs resulting in the release of OH^- ions. These OH^- ions subsequently interact with Ca^{2+} present in α -HPG, eliciting a reaction that leads to the formation of $\text{Ca}(\text{OH})_2$. The emergence of $\text{Ca}(\text{OH})_2$ enhances the surface concentration of hydroxyl groups on α -HPG.¹³ When Na_2SO_4 is dissolved in water, SO_4^{2-} is produced, and SO_4^{2-} can combine with Ca^{2+} in α -HPG to form CaSO_4 , which contributes to the forward progress of reaction 5. And Na^+ in Na_2SO_4 reacts with CaSO_4 in phosphogypsum to form water-soluble $\text{CaSO}_4 \cdot \text{Na}_2\text{SO}_4$, as shown in reaction 6, and this water-soluble product helps to improve the reactivity and solubility of α -HPG.



In summary, the combined influence of optimal proportions of NaOH and Na_2SO_4 synergistically augments the surface hydroxyl group count on α -HPG in a more efficacious manner, and the increased hydroxyl groups can improve the reactivity of α -HPG and make it easier to react with other substances.

3.4. Effect of Hydroxylation on the Properties of α -HPG. **3.4.1. XRD Analysis.** Figure 3 shows the XRD spectra of α -HPG and $\text{OH-}\alpha$ -HPG. α -HPG is mainly composed of $\text{CaSO}_4 \cdot 0.5\text{H}_2\text{O}$ (PDF#41-0224, space group $I2(S)$) and SiO_2 (PDF#70-2536, space group $P3221$). In the XRD spectra of α -HPG, the major diffraction peaks with 2θ values of 14.7°,

Table 1. Compositional Analysis of HPG

samples	SO_3	CaO	SiO_2	P_2O_5	Al_2O_3	Fe_2O_3	KO_2	TiO_2	CeO_2	Cl	SrO	ZnO
α -HPG	56.531	38.316	2.588	1.146	0.610	0.412	0.135	0.100	0.046	0.027	0.023	0.005
β -HPG	53.456	40.656	2.925	1.088	0.645	0.574	0.185	0.111	0.107	0.024	0.032	0.005

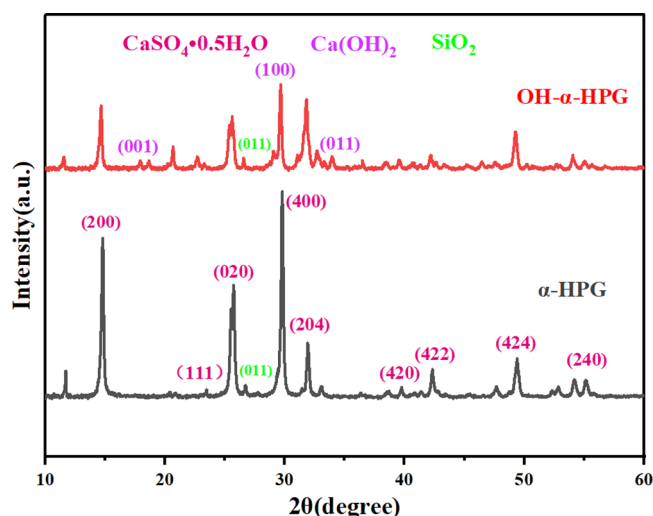


Figure 3. XRD patterns of different α -HPG samples.

23.42°, 25.7°, 26.7°, 29.8°, 32.0°, 39.7°, 42.3°, 49.4°, and 55.2° correspond to (200), (111), (020), (011), (400), (204), (420), (422) and (240). Within the XRD spectra of OH- α -HPG, the diffraction peak associated with the $\text{CaSO}_4 \cdot 0.5\text{H}_2\text{O}$ crystal plane (400) exhibits the most pronounced intensity, whereas the peak at a 2θ value of 26.7° corresponds to the primary diffraction feature of the SiO_2 (011) crystal plane, the main diffraction peaks of $\text{Ca}(\text{OH})_2$ at 2θ values of 18.2°, 29.7°, and 34.1° corresponded to the (001), (100), and (011) crystal planes, respectively. This phenomenon arises from the interaction between sodium hydroxide and Ca^{2+} ions present in HPG, leading to the formation of $\text{Ca}(\text{OH})_2$ that subsequently precipitates onto the surface of α -HPG. In addition, the diffraction peak intensities of α -HPG were stronger, especially at the crystal surface (020), compared to OH- α -HPG. This was attributed to the fact that $\text{Ca}(\text{OH})_2$ formed during the reaction process was deposited on the surface of α -HPG, which significantly increased the number of surface hydroxyl groups, as shown in the reaction equation in 5.

3.4.2. FTIR Analysis. The infrared spectrum of α -HPG depicted in Figure 4 reveals characteristic peaks at 3610 and 3550 cm^{-1} , which are ascribable to the symmetric stretching

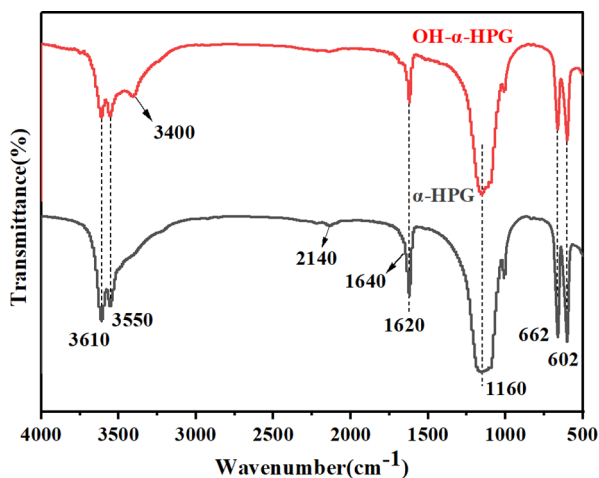


Figure 4. FTIR spectra of different α -HPG samples.

vibrations of the crystalline water molecules within $\text{CaSO}_4 \cdot 2\text{H}_2\text{O}$. Furthermore, the peaks in the vicinity of 1640 and 1620 cm^{-1} signify the bending vibrations of the same crystalline water. The presence of peaks at 662 and 602 cm^{-1} are indicative of the antisymmetric bending vibrations of SO_4^{2-} ions. Notably, a broad peak centered at 2140 cm^{-1} indicates the establishment of hydrogen bonds between hydroxyl groups residing on the α -HPG surface and other molecular entities. This hydrogen bonding results in a red shift of the hydroxyl stretching vibration peak from its typical position at 3400 to 2140 cm^{-1} , owing to a reduction in system energy. Consequently, the intensity of the hydroxyl stretching vibration peak at 3400 cm^{-1} in the α -HPG spectrum is notably low, corroborating the limited presence of hydroxyl groups on its surface. In contrast, the spectrum of OH- α -HPG exhibits a more intense hydroxyl stretching vibration peak at 3400 cm^{-1} , indicating a substantial increase in the hydroxyl group density on the α -HPG surface following hydroxylation. Additionally, the deposition of $\text{Ca}(\text{OH})_2$ on the α -HPG surface leads to a decrease in the intensity of the asymmetric stretching vibration peak of SO_4^{2-} at 1160 cm^{-1} , which aligns with the emergence of new $\text{Ca}(\text{OH})_2$ diffraction peaks observed in the XRD pattern of OH- α -HPG.

3.5. TG Analysis. Figure 5 shows the thermogravimetric curves of α -HPG before and after modification. In the

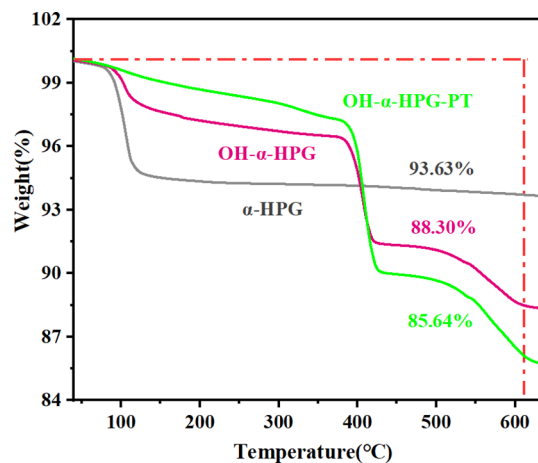


Figure 5. TG curves of different α -HPG samples.

temperature range of 0–90 °C, all three α -HPG samples exhibited a trace amount of thermal weight loss, this observation can be attributed to the elimination of interstitial water molecules from the $\text{CaSO}_4 \cdot 2\text{H}_2\text{O}$ crystal lattice. Subsequently, given that the onset temperature for the initial decomposition of CaSO_4 is notably high, ranging from 1000 to 1200 °C, there was virtually no thermal weight loss of the α -HPG samples over the temperature range of 140 to 650 °C, and less than 6.37% weight loss over the 650 °C temperature range. The weight loss of OH- α -HPG in the temperature range of 90–650 °C was 11.7%, with the temperature in the 370 ~ 440 °C range had the highest decomposition rate. This phenomenon can be attributed to the partial decomposition of $\text{Ca}(\text{OH})_2$ that has accumulated on the surface of OH- α -HPG, thereby reinforcing the evidence for the successful hydroxylation treatment applied to the α -HPG surface. The weight loss of OH- α -HPG-PT reached 14.36%. The initial stage of thermal mass loss can be ascribed to the decomposition of the free proton reaction byproducts, which are generated by the

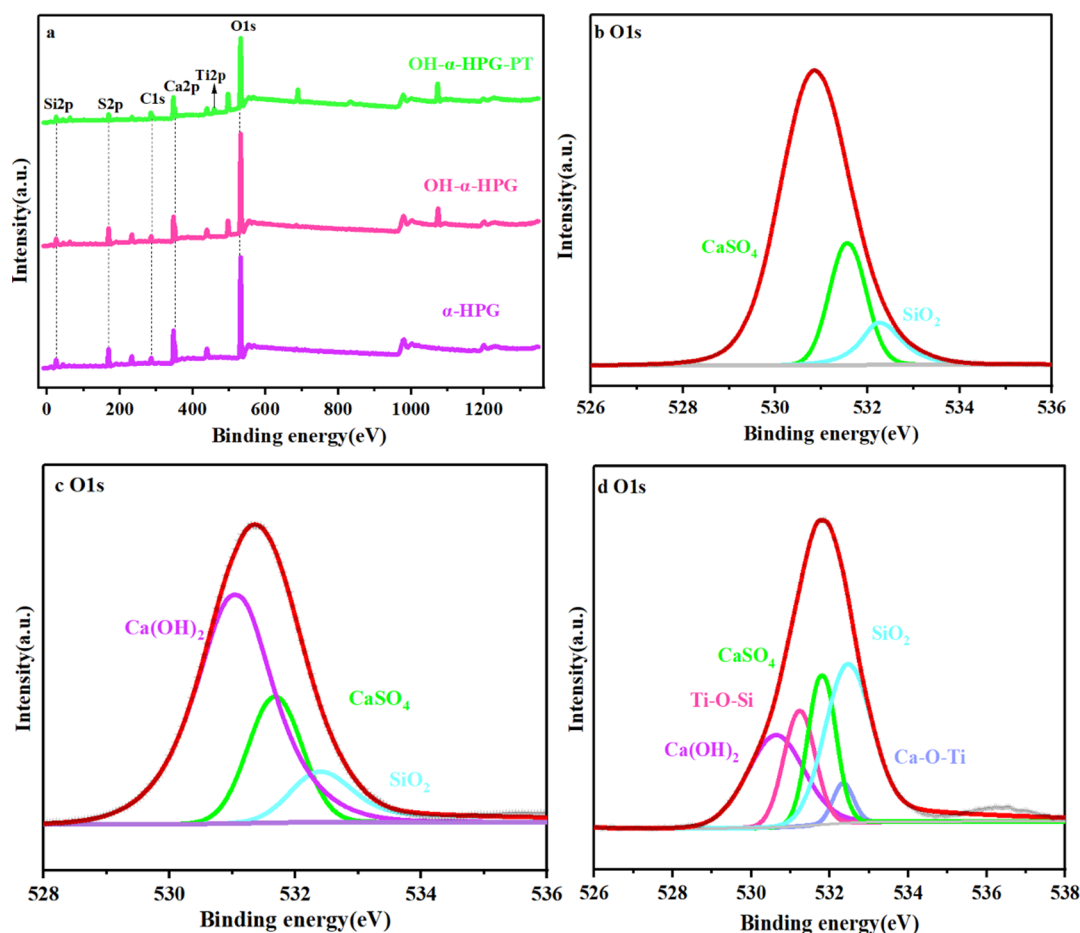


Figure 6. Comprehensive survey XPS spectra (a) and O 1s spectra of α -HPG (b), OH- α -HPG (c), and OH- α -HPG-PT (d).

PT process occurring on the OH- α -HPG surface. The temperature range of the highest decomposition rate was 380 \sim 440 $^{\circ}$ C. The second stage primarily encompassed the thermal degradation of the unreacted Ca(OH)₂ and the grafted organic chains present on the surface of OH- α -HPG-PT. As a result, the grafting rates of PT on the α -HPG and OH- α -HPG surfaces were 2.65 and 7.89 wt %, respectively, which indicated that hydroxylating α -HPG significantly increased the grafting rate of PT on the OH- α -HPG surface.

3.6. XPS Analysis. As depicted in Figure 6a, the intensity of the S 2p peaks for both OH- α -HPG and OH- α -HPG-PT is notably weaker in comparison to that of α -HPG, whereas the intensity of the C 1s peaks experiences a marked augmentation. This observation can be attributed to the fact that a portion of the CO₂ present in the air is capable of being adsorbed onto the surface of α -HPG. When α -HPG is hydroxylated with NaOH and Na₂SO₄, the generated Ca(OH)₂ will be deposited on the surface of α -HPG, which adsorbs a small amount of CO₂, leading to the increase of carbon content and the enhancement of peaks. In addition, the long carbon chain siloxane of PT also contributes to the increase of carbon content. As a result, OH- α -HPG-PT shows the highest carbon peak intensity, which is attributed to OH- α -HPG-PT being wrapped by long carbon chain organosiloxanes leading to the

The qualitative and quantitative analysis of the surface elemental composition of α -HPG samples subjected to varying treatment methodologies was conducted, and the experimental outcomes are presented in Figure 6 and Table 2. The predominant elements identified in α -HPG, OH- α -HPG, and

Table 2. Content of Various Elements in Different α -HPG Samples

samples	elemental content (%)					
	C	O	S	Ca	Si	Ti
α -HPG	11.48	60.75	13.69	12.39	1.69	0
OH- α -HPG	11.40	63.84	13.07	10.11	1.57	0
OH- α -HPG-PT	21.27	57.65	6.1	9.61	2.84	2.53

OH- α -HPG-PT comprised of O, C, S, Ca, Si, and Ti. When compared to α -HPG (Si content: 1.69%) and OH- α -HPG (Si content: 1.57%), the Si content on the surface of the OH- α -HPG-PT samples increased significantly to 2.84%. This is consistent with the analysis of the XRD pattern of α -HPG, indicating that SiO₂ is an impurity. After hydroxylation, the decrease in silicon content to 1.57% in OH- α -HPG can be attributed to the deposition of Ca(OH)₂ on the surface of α -HPG. On the contrary, the Si content in OH- α -HPG-PT increased to 2.84%, which was significantly higher than that in α -HPG, indicating that the PT hydrophobic modifier branched the organic links on the surface of OH- α -HPG. The C content in OH- α -HPG-PT was 21.27%, which was significantly higher than that of other α -HPG samples due to the longer organic carbon chains in PT. The Ti content in OH- α -HPG-PT was 2.53%, which was attributed to the adsorption of TiO₂ nanoparticles and organic carbon chains from PT hydrophobic modifier on the surface of OH- α -HPG samples. In the O 1s XPS spectrum of α -HPG depicted in Figure 6b, the peak observed at 531.80 eV is attributed to the interaction between

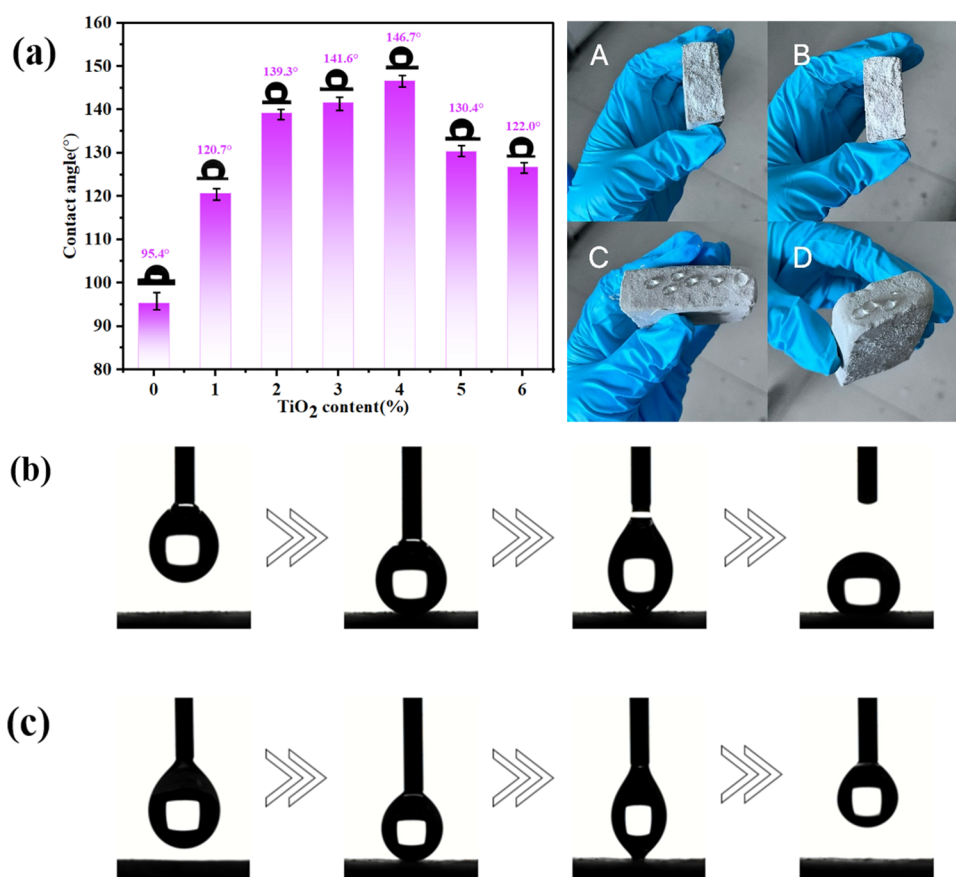


Figure 7. (a) Relationship between TiO₂ mass fraction and water contact angle and comparison of surface hydrophobicity of OH- α -HPG -PT with control. (b) The contact and detachment process of water droplets on the surface of OH- α -HPG -PFDTS. (c) The contact and detachment process of water droplets on the surface of OH- α -HPG -PT.

Ca²⁺ and SO₄²⁻, whereas the peak at 532.5 eV stems from SiO₂ impurities.³³ Conversely, in the O 1s XPS spectrum of OH- α -HPG shown in Figure 6c, the peak located at 530.8 eV is attributed to the deposition of Ca(OH)₂ on the surface of α -HPG, which arises from the reaction between NaOH and CaSO₄ during the hydroxylation process. In Figure 6d, the intensity of the peak at 530.8 eV is lower than that in Figure 6c, which is since some hydroxyl groups in the OH- α -HPG samples were consumed during the condensation reaction with the PT hydrophobic modifier. In Figure 6d, the peaks at 531.3 and 532.4 eV within the O 1s spectra of OH- α -HPG-PT correspond to oxygen atoms residing in the Ti–O–Si and Ca–O–Ti bonds, respectively. Therefore, the XPS further confirmed that the α -HPG samples were modified by hydroxylation with PT hydrophobic agent surface modification, which formed Ti–O–Si and Ca–O–Ti bonds on their surfaces, and the α -HPG samples obtained excellent hydrophobicity.

3.7. Surface Wettability Analysis. 3.7.1. Contact Angle and Adhesion Analysis. In our previous study, the peak contact angle of hydrophobic coatings formulated with toluene-synthesized organic/inorganic composite hydrophobes was 148.7°, which was slightly higher than that of coatings formulated with ethanol, which was 146.7°. However, toluene possesses a higher toxicity profile in comparison to ethanol. Employing ethanol as a solvent not only mitigates environmental pollution but also expedites the drying process of surface hydrophobic coatings. Therefore, in this study, a PT hydrophobic modifier consisting of PFDTS and TiO₂ nano-

particles was prepared by solution polymerization using ethanol as a solvent. Figure 7a shows the relationship between the mass fraction of TiO₂ and the water contact angle, as well as the comparison of the surface hydrophobicity of OH- α -HPG -PT with that of the control. As shown in Figure 7a, upon maintaining a constant concentration of PFDTS, the contact angle initially exhibited an upward trend followed by a decline as the mass fraction of TiO₂ was increased. When the mass fraction of TiO₂ was 0, 1, 2, 3, 4, 5, and 6%, the corresponding contact angles were 95.4°, 120.7°, 139.3°, 141.6°, 146.7°, 130.4° and 122.0°, respectively. The maximum contact angle was 146.7° when the mass fraction of TiO₂ was 4%. Excessive amount of TiO₂ nanoparticles leads to incomplete reaction of PFDTS with nanoparticles, so it is necessary to minimize the use of TiO₂ nanoparticles. As shown in the α -HPG samples (A and B) in Figure 7a, when a water droplet is put inside the α -HPG sample, the water droplet directly wets the α -HPG sample with very poor hydrophobicity. In contrast, when the hydroxylated α -HPG samples were modified with a PT composite hydrophobic modifier with a mass fraction of 4% good hydrophobicity could be obtained, as shown in the OH- α -HPG -PT samples (C and D) in Figure 7a, which was attributed to the fact that the PT composite hydrophobic modifier bonded with OH- α -HPG to form a hydrophobic silicone network structure, which reduced the porosity of OH- α -HPG that improves the hydrophobicity of the OH- α -HPG samples.

Figure 7b,c compare the process of adhesion change of hydrophobic coating on the surface of OH- α -HPG-PFDTS

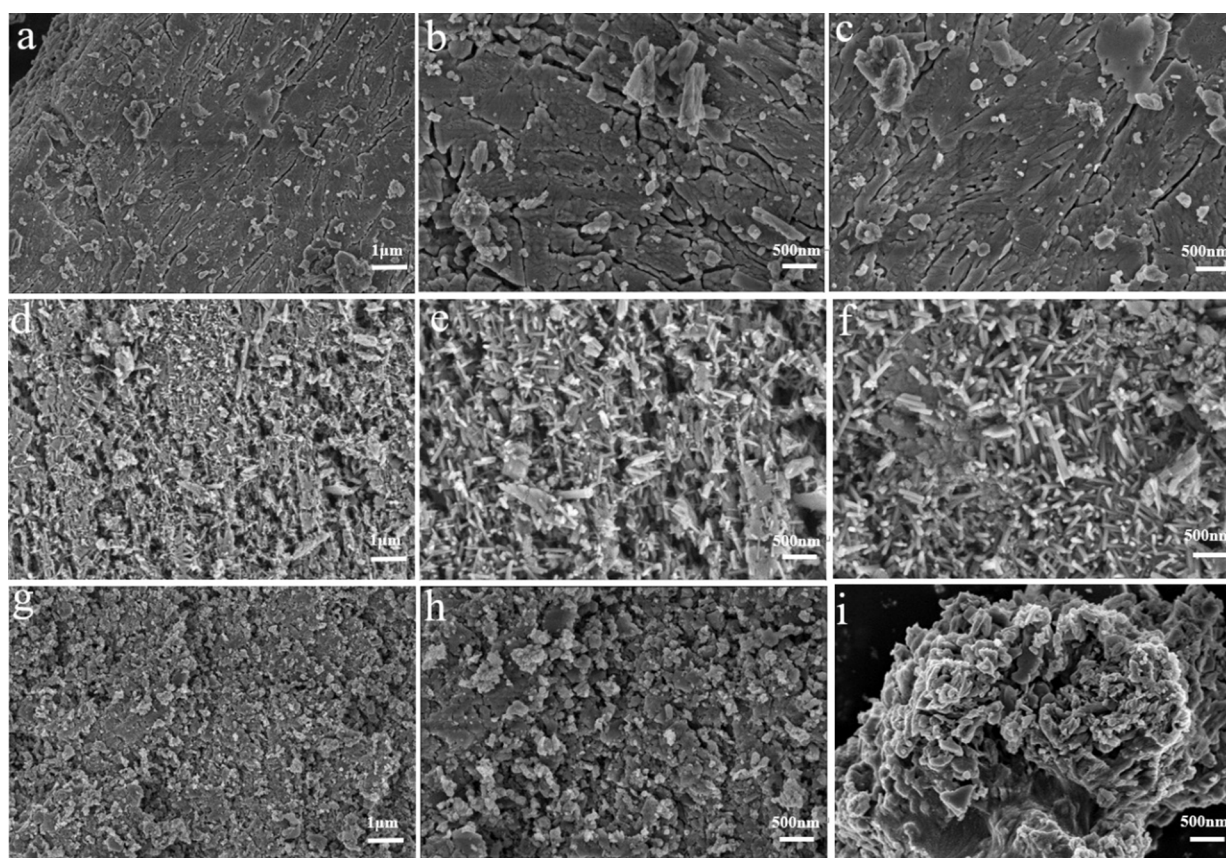


Figure 8. SEM images of the surface of different α -HPG samples. (a–c) α -HPG, (d–f) OH- α -HPG, (g–i) OH- α -HPG-PT images at different magnifications.

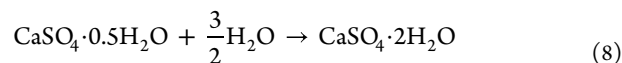
samples with and without TiO₂ nanoparticles. Under the influence of TiO₂ nanoparticles, a transition from high adhesion to low adhesion was realized. The schematic diagram in Figure 7c explains this phenomenon.

Quantifying Adhesion Functions Using the Young-Dupre Equation:³⁴

$$W_{LS} = r_L(1 + \cos\theta) \quad (7)$$

Herein, W_{LS} signifies the adhesion work required to fully detach the water droplet from the hydrophobic surface, with L and S representing the liquid and solid phases, respectively. Given that the surface tension of the water droplet r_L is 72 mN m⁻¹ at room temperature (25 °C), and θ represents the contact angle. The adhesion force of the α -HPG hydrophobic surface was determined to be 0.013677 J m⁻², assuming a contact angle of 146.7°. This value underscores the exceedingly low adhesion force exhibited by this hydrophobic surface.

3.8. Surface Microstructure Analysis. As depicted in reaction 8, α -HPG undergoes hydration to form elongated rod-shaped CaSO₄·2H₂O crystal structures, which exhibit a loosely interlocked arrangement, characterized by a significant porosity. This porous structure allows for the infiltration of water, generating bidirectional pressures that subsequently induce internal stresses within the α -HPG matrix. In addition, water can dissolve the crystallization contact points of α -HPG hardened body, causing it to recrystallize and reduce its mechanical properties.³⁵ Thus, macroscopically, this indicates a decrease in the softening coefficient and an increase in water absorption.



As shown in Figure 8a–c, the unhydroxylated α -HPG surface is dominated by long rod-like crystals of CaSO₄·2H₂O. The α -HPG surface is also characterized by a high degree of hydroxylation. Upon completion of the hydroxylation and subsequent reaction described in eq 5, the rod-shaped crystals present on the α -HPG surface underwent a morphological transformation into needle-like crystals, as evident in Figure 8d–f. Concurrently, a deposition process of Ca(OH)₂ occurred on the α -HPG surface. The augmentation in the length-to-diameter ratio of the OH- α -HPG crystals, coupled with an increase in intercrystalline porosity and specific surface area, facilitated the creation of more reactive sites for the subsequent synthesis of polysiloxane-hybridized nanoparticles on the OH- α -HPG coating surface, thereby enhancing its reactivity potential.

The microstructural features of the OH- α -HPG-PT sample's surface are illustrated in Figure 8g–i. After hydrophobic modification of α -HPG by combining PFDTS and TiO₂, it can be observed that the crystals on the surface of the α -HPG samples were transformed from needle-like interconnections to fine particles. This suggests that the cross-linking between PFDTS and TiO₂ results in the formation of a hydrophobic layer on the α -HPG surface, facilitated by hydrogen bonding interactions. As the hydrogen bonds between PFDTS, TiO₂ and the α -HPG surface catalyze and cross-link each other to generate a hydrophobic network structure and deposit on the α -HPG surface, a hydrophobic barrier is formed. The incorporation of TiO₂ nanoparticles into the hydrophobic

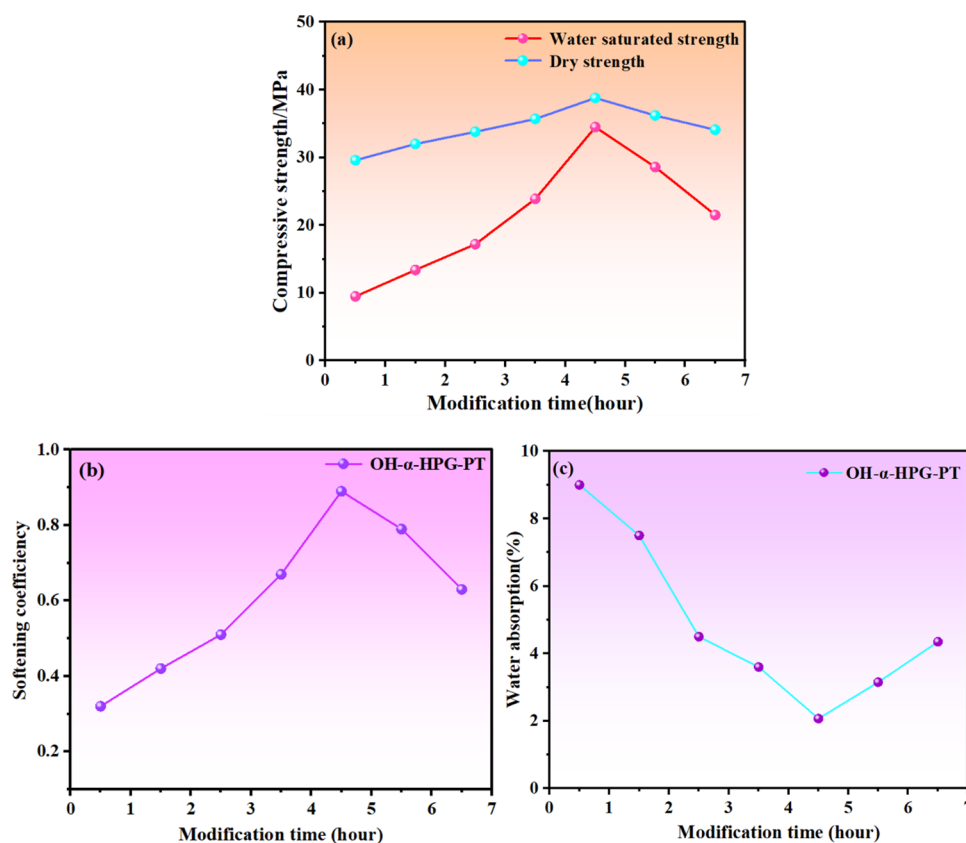


Figure 9. (a) Effect of different modification times on the compressive strength of α -HPG; (b) effect of different modification times on the softening coefficient of α -HPG; (c) effect of different modification times on the water absorption of α -HPG.

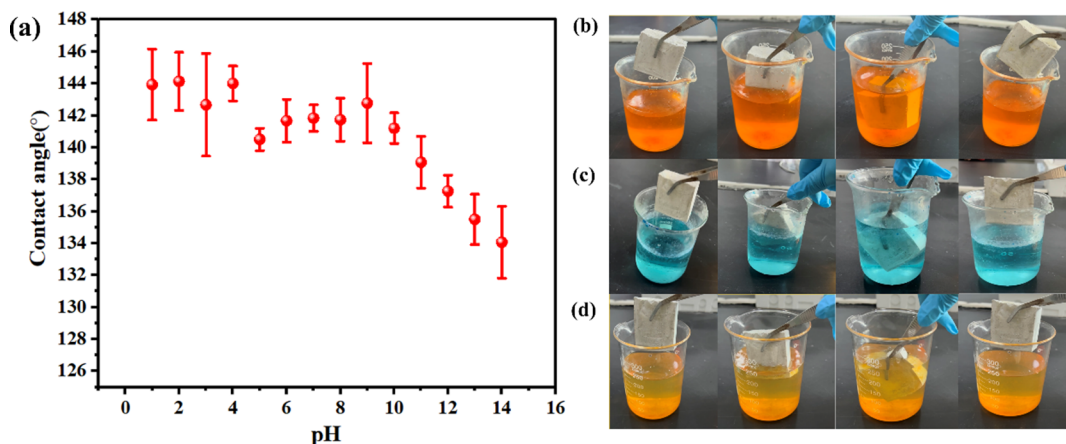


Figure 10. (a) Surface chemical stability of OH- α -HPG-PT, (b–d) photographs of OH- α -HPG-PT immersed in methyl orange-stained HCl solution (pH = 1), MB (methylene blue)-stained deionized water (pH = 7), and rhodamine 6G-stained NaOH solution (pH = 14).

coatings further diminishes their surface energy, fills up the pores of the hemihydrated crystals, and decreases the porosity of the α -HPG and enhances its hydrophobicity.

3.9. Effect of PT Hydrophobic Modifier on OH- α -HPG Properties. The graph in Figure 9a depicts the correlation between the compressive strength and the duration of the modification process. The compressive strength increased significantly with the increase of modification time and decreased gradually after reaching the peak value. 4.5 h as the optimal modification time, the dry compressive strength and water-saturated compressive strength reached 38.8 and 34.5 MPa, respectively. However, further increase of the

modification time decreases the compressive strength of OH- α -HPG samples. This is because when modifying the OH- α -HPG samples in the PT hydrophobic agent for too long, the PT hydrophobic agent decreases the densification of the crystal structure of phosphogypsum of the OH- α -HPG samples during the hydration process. Therefore, 4.5 h was taken as the optimal modification time for OH- α -HPG samples. The dependence of the softening coefficient on the modification time is presented in Figure 9b, where a notable increase in the softening coefficient is observed with an extension in the modification duration, reaching a peak value before gradually declining. The softening coefficient reaches a maximum value

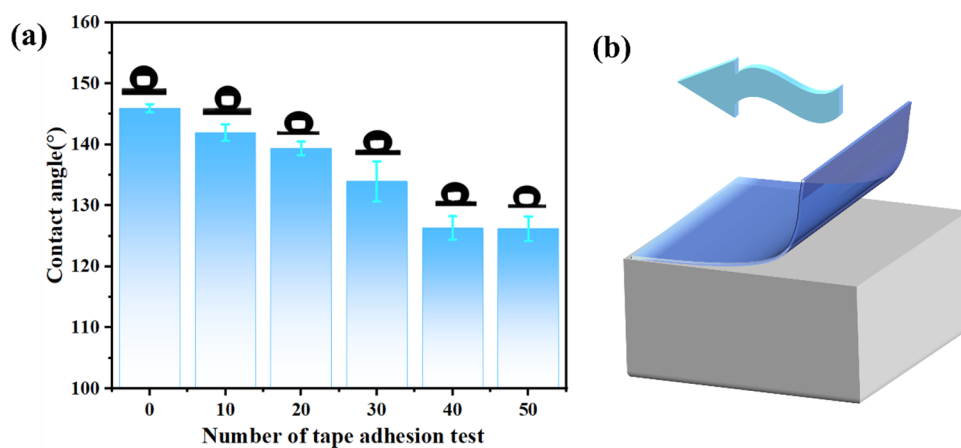


Figure 11. (a,b) OH- α -HPG-PT tape adhesion peeling experiment.

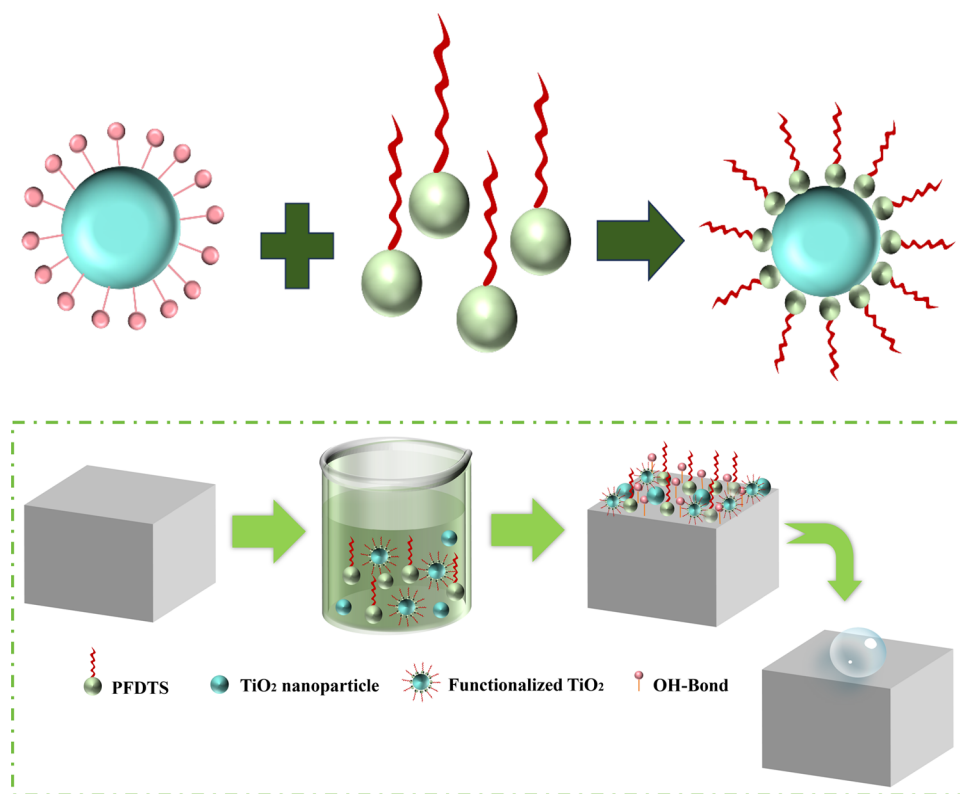


Figure 12. Reaction mechanism of surface hydrophobic modification on OH- α -HPG samples.

of 0.89 when OH- α -HPG is modified by PT hydrophobicity for 4.5 h. α -HPG is classified as a member of the tripartite crystal system, characterized by the presence of intrinsic pores and capillary channels within its structure.³⁶ The notable enhancement in the softening coefficient of the modified OH- α -HPG samples can be attributed to the development of micron/nanoscale hierarchical roughness on their surfaces, which serves as a barrier to impede water penetration into the interior of the samples. As depicted in Figure 9c, the relationship between water absorption and modification time reveals a significant decrease in water absorption with an increase in modification duration, attaining a minimum value before gradually rising. Notably, when the OH- α -HPG samples underwent hydrophobic modification with PT for 4.5 h, a minimal water absorption rate of 2.07% was achieved, suggesting the efficacy of the PT composite hydrophobic

modifier in effectively mitigating the water absorption of OH- α -HPG samples.

4. STABILIZATION OF HYDROPHOBIC COATINGS ON OH- α -HPG SURFACES

4.1. Strong Acid and Alkali Corrosion Test. Chemical stability emerges as a pivotal criterion in assessing the hydrophobic nature of α -HPG surfaces. To validate the resilience of OH- α -HPG-PT in retaining hydrophobicity across a defined spectrum of acidic and alkaline environments, an investigation was conducted to assess the contact angles of OH- α -HPG-PT in solutions spanning a pH range from 1 to 14. As illustrated in Figure 10a, the contact angle remained above 140° within the pH range of 1 to 10, indicative of robust hydrophobicity. Within the alkaline region of pH 11 to 14,

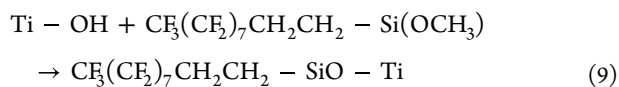
although the contact angle declined below 140° , it remained above 132.3° , leading to the inference that this reduction was attributable to the partial dissolution of TiO_2 nanoparticles in the alkaline medium.³⁷

As depicted in Figure 10b–d, the surface of OH- α -HPG-PT remained visibly dry and unaffected by water wetting, even after being extracted from dyeing solutions with varying pH values using tweezers, thereby substantiating its exceptional chemical stability. Upon immersion in dyeing solutions, OH- α -HPG-PT exhibited a “mirror” effect, stemming from the ultralow surface energy of its coating. This phenomenon is attributed to the formation of “air valleys,” or an air layer, prior to the contact between PFDTs/nano- TiO_2 and the ambient air, effectively barring further interaction between water and the phosphogypsum surface. Further contact with the phosphogypsum surface³⁸ This is due to the “air valley”, i.e. the air layer, which prevents further contact between water and the phosphogypsum surface. Pursuant to the Cassie–Baxter theory,³⁹ the presence of an air layer at a liquid–solid interface characterized by low surface energy induces a reversed Laplace pressure, culminating in the levitation of liquid droplets atop the roughened solid surface. The augmentation in the thickness of this air layer at the solid–liquid interface facilitates the establishment of a discrete solid–liquid–gas three-phase contact interface, thereby reducing the energy threshold for droplet rolling and enhancing the feasibility of constructing hydrophobic surfaces.

4.2. Tape Adhesion and Peeling Test. The tape adhesion peel-off test constitutes a reliable methodology for evaluating the mechanical robustness of hydrophobic coatings. Figure 11b illustrates a schematic representation of the experimental protocol, entailing the initial gentle application of an adhesive tape to adhere to the OH- α -HPG-PT surface, followed by rolling the tape over the designated test area with weights at a consistent and uniform velocity. Subsequently, the tape is peeled off, and the surface is gently blown with a washout ball to assess the contact angle, thereby quantifying the coating’s mechanical integrity. As shown in Figure 11a, after 50 adhesion experiments, the OH- α -HPG-PT surface still maintained a contact angle of 124.2° .

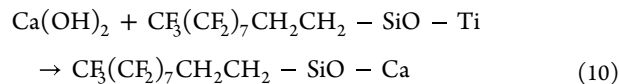
5. MECHANISM OF HYDROPHOBIC MODIFICATION OF OH- α -HPG SURFACE

Figure 12 depicts the mechanistic pathway for the formation of a hydrophobic coating on the OH- α -HPG surface. Typically, the surface of TiO_2 nanoparticles is adorned with a layer of hydroxyl groups. Upon blending TiO_2 nanoparticles with a PFDTs solution, the hydrophilic $\text{CF}_3(\text{CF}_2)_7\text{CH}_2\text{CH}_2\text{-SiO-}$ moiety within PFDTs engages in a reaction (as depicted in reaction 9), leading to the displacement of the hydroxyl groups on the TiO_2 surface. Subsequently, these $\text{CF}_3(\text{CF}_2)_7\text{CH}_2\text{CH}_2\text{-SiO-}$ groups attach to the TiO_2 surface via hydrogen bonding interactions. Given the continuous nature of this process, a self-assembled monolayer of $\text{CF}_3(\text{CF}_2)_7\text{CH}_2\text{CH}_2\text{-SiO-}$ is formed, encapsulating the entire TiO_2 surface, thereby imparting hydrophobic functionality to the nanoparticles.²⁰



After the functionalization of TiO_2 nanoparticles is completed, the remaining PFDTs molecules remain unreacted in the solution. Upon immersion of the hydroxylated α -HPG

sample in the PFDTs + TiO_2 solution, an initial reaction occurs between the unreacted PFDTs molecules, and the Ca(OH)_2 residue present on the α -HPG surface, as illustrated in reaction 10.



The $\text{CF}_3(\text{CF}_2)_7\text{CH}_2\text{CH}_2\text{-SiO-}$ monomers present in solution undergo self-assembly to form monolayers on the surface of α -HPG, facilitated by hydrogen bonding interactions. This mechanism is analogous to the one proposed by Yu et al.⁴⁰ in their synthesis of α -HPG. A similar mechanism was proposed in the preparation of superhydrophobic aluminum surfaces using PFDTs. Subsequently, TiO_2 nanoparticles functionalized with PFDTs were deposited on the monolayer formed on the α -HPG surface as shown in Figure 10. Functionalized TiO_2 nanoparticles and hydrophobic PFDTs monolayer $\text{CF}_3(\text{CF}_2)_7\text{CH}_2\text{CH}_2\text{-SiO-}$ were deposited on the phosphogypsum surface by chemisorption.⁴¹

6. CONCLUSIONS

In this study, the hydroxylation treatment and surface hydrophobic modification of α -HPG were investigated. The chemical composition of the α -HPG surface and the hydrophobic characteristics of OH- α -HPG-PT composites were scrutinized utilizing diverse analytical methodologies. Drawing upon the findings presented in this study, the key conclusions can be summarized as follows:

1. The hydroxylation process of the α -HPG surface serves to augment the density of hydroxyl groups present on its exterior, thereby enhancing the efficacy of the grafting reaction with hydrophobic modifiers. The grafting rates of hydrophobic modifier PFDTs+ TiO_2 on the surfaces of α -HPG samples and OH- α -HPG samples were 2.65 and 7.89 wt %, respectively. The grafting rates of PT composite hydrophobic modifier on the surfaces of OH- α -HPG samples were significantly increased, indicating that the hydrophobicity of α -HPG samples was significantly increased.
2. In this study, the surface hydrophobicity modification of α -HPG was mainly realized by impregnation method. The siloxane moieties of PFDTs, the hydroxyl functionalities residing on the TiO_2 nanoparticle surface, along with the Ca(OH)_2 produced via the hydroxylation reaction, collectively interacted with the hydroxyl groups present on the α -HPG surface. The groups on the surface of phosphogypsum were transformed from -OH to long organic chains, so that the hydrophobic network structure was tightly adsorbed on the surface of α -HPG samples by chemisorption, thus enhancing its hydrophobicity.
3. In the comparative experimental setup, 0.01% (v/v) of PFDTs was dissolved in a 20 mL ethanol solvent medium, it was found that the PT composite hydrophobic modifier prepared by adding 0.8 g of TiO_2 nanoparticles effectively modified the OH- α -HPG samples after 4.5 h of modification, and the dry and water-saturated compressive strengths could reach a maximum of 38.8 and 34.5 MPa, respectively, and the softening The softening coefficient was as high as 0.89,


the water absorption rate was as low as 2.07%, and the contact angle reached the maximum value of 146.7°.

- OH- α -HPG-PT has excellent chemical stability, the contact angle is still not less than 132.3° under strong acid or alkali conditions. Following 50 iterations of the tape adhesion test, the contact angle remained at 123.7°. Similarly, after undergoing 100 abrasion tests, the contact angle persisted at 124.2°.

Therefore, the PFDTs/TiO₂ hydrophobic coating prepared on the surface of OH- α -HPG samples by impregnation method has a promising application in the field of building materials. This research holds significant implications for the exploration of phosphogypsum resource utilization and the surface modification of inorganic fillers.

AUTHOR INFORMATION

Corresponding Author

Qibin Liu – School of Materials and Metallurgy, Guizhou University, Guiyang 550025, China;  orcid.org/0000-0003-4387-4149; Email: qbliugzu@163.com

Authors

Yuanxia Li – School of Materials and Metallurgy, Guizhou University, Guiyang 550025, China

Fangfang Zeng – School of Materials and Metallurgy, Guizhou University, Guiyang 550025, China

Guang Yang – School of Materials and Metallurgy, Guizhou University, Guiyang 550025, China

Yi Li – School of Materials and Metallurgy, Guizhou University, Guiyang 550025, China

Shun Zhang – School of Materials and Metallurgy, Guizhou University, Guiyang 550025, China

Complete contact information is available at:

<https://pubs.acs.org/10.1021/acsomega.4c04735>

Notes

The authors declare no competing financial interest.

REFERENCES

- Ding, W.; Chen, Q.; Sun, H.; Peng, T. Modified mineral carbonation of phosphogypsum for CO₂ sequestration. *Journal of CO₂ Utilization* **2019**, *34*, 507.
- Chuan, L. M.; Zheng, H. G.; Zhao, J. J.; Wang, A. L.; Sun, S. F. Phosphogypsum production and utilization in China. *IOP Conf. Ser.: Mater. Sci. Eng.* **2018**, *382* (2), No. 022099.
- Costa, A. R. D.; Matos, S. R. C.; Camarini, G.; Gonçalves, J. P. Hydration of sustainable ternary cements containing phosphogypsum. *Sustainable Mater. Technol.* **2021**, *28*, No. e00280. Feng, L.; Jin, K.; Wang, H. Research on the Thermal Conductivity and Water Resistance of Foamed Phosphogypsum. *Coatings* **2021**, *11*, 802.
- Wu, F.; Yang, C.; Qu, G.; Liu, L.; Chen, B.; Liu, S.; Li, J.; Ren, Y.; Yang, Y. Study of Semi-Dry High Target Solidification/Stabilization of Harmful Impurities in Phosphogypsum by Modification. *Molecules* **2022**, *27*, 462.
- Wu, F.; Ren, Y.; Qu, G.; Liu, S.; Chen, B.; Liu, X.; Zhao, C.; Li, J. Utilization path of bulk industrial solid waste: A review on the multi-directional resource utilization path of phosphogypsum. *Journal of Environmental Management* **2022**, *313*, 114957.
- Yang, J.; Liu, S.; Wang, Y.; Huang, Y.; Yuxin, S.; Dai, Q.; Liu, H.; Ma, L. Phosphogypsum Resource Utilization Based on Thermodynamic Analysis. *Chem. Eng. Technol.* **2022**, *45*, 776–790.
- Rashad, A. M. Phosphogypsum as a construction material. *Journal of Cleaner Production* **2017**, *166*, 732.
- Kondratieva, N.; Barre, M.; Goutenoire, F.; Sanytsky, M. Study of modified gypsum binder. *Construction and Building Materials* **2017**, *149*, 535.
- Zhou, J.; Zhang, Y.; Shu, Z.; Wang, Y.; Yakubu, Y.; Zhao, Y.; Li, X. Enhancing waterproof performance of phosphogypsum non-fired ceramics by coating silane-coupled unsaturated polyester resin. *Mater. Lett.* **2019**, *252*, 52.
- Deng, Y.; Xuan, L.; Feng, Q. Effect of a waterproof agent on gypsum particleboard properties. *Holzforchung* **2006**, *60*, 318.
- Liu, J.; Hu, L.; Tang, L.; Zhang, E. Q.; Ren, J. FShrinkage behaviour, early hydration and hardened properties of sodium silicate activated slag incorporated with gypsum and cement. *Construction and Building Materials* **2020**, *248*, 118687.
- Wang, Q.; Wang, D.; Chen, H. The role of fly ash microsphere in the microstructure and macroscopic properties of high-strength concrete. *Cement and Concrete Composites* **2017**, *83*, 125. Wang, Q.; Wang, D.; Zhuang, S. The soundness of steel slag with different free CaO and MgO contents. *Construction and Building Materials* **2017**, *151*, 138.
- Chen, Y.; Ding, Y.; Dong, Y.; Liu, Y.; Ren, X.; Wang, B.; Gao, C. Surface modification of calcium sulfate whisker using thiol-ene click reaction and its application in reinforced silicone rubber. *J. Polym. Sci.* **2020**, *58*, 624. Lan, S.; Li, L.; Xu, D.; Zhu, D.; Liu, Z.; Nie, F. Surface modification of magnesium hydroxide using vinyltriethoxysilane by dry process. *Appl. Surf. Sci.* **2016**, *382*, 56. Li, C. Q.; Liang, C.; Chen, Z. M.; Di, Y. H.; Zheng, S. L.; et al. Surface modification of calcium carbonate: A review of theories, methods and applications. *J. Cent. South Univ.* **2021**, *28*, 2589–2611. Lin, T.; Du, J.; Liu, L.; Wu, Z.; Kong, X.; Liu, Y.; Cai, Y. Treatment with Minocycline Suppresses Microglia Activation and Reverses Neural Stem Cells Loss after Simulated Microgravity. *BioMed. Research International* **2020**, *2020*, 1. Zhu, D.; Nai, X.; Lan, S.; Bian, S.; Liu, X.; Li, W. Surface modification of magnesium hydroxide sulfate hydrate whiskers using a silane coupling agent by dry process. *Appl. Surf. Sci.* **2016**, *390*, 25.
- Liu, H.; Nie, C.; Li, H.; Xie, G.; Cao, J. Hydrophobically modified phosphogypsum and its application in polypropylene composites. *Construction and Building Materials* **2022**, *347*, 128500.
- Chen, H. Y.; Wang, J.; Ma, P. Y.; Liang, J.; Xiang, L. Influence of hydroxylation on fabrication of PVC/CaSO₄ composite. *Appl. Surf. Sci.* **2015**, *357*, 2320–2326.
- Gonçalves, G.; Marques, P. A. A. P.; Barros-Timmons, A.; Bdkin, I.; Singh, M. K.; Emami, N.; Grácio, J. Graphene oxide modified with PMMA via ATRP as a reinforcement filler. *J. Mater. Chem.* **2010**, *20* (44), 9927.
- Lu, Y.; Jiang, N.; Li, X.; Xu, S. Effect of inorganic–organic surface modification of calcium sulfate whiskers on mechanical and thermal properties of calcium sulfate whisker/poly(vinyl chloride) composites. *RSC Adv.* **2017**, *7* (73), 46486–46498.
- Liu, X.; Bai, Y.; Xu, J.; Xu, Q.; Xiao, L.; Sun, L.; Weng, J.; Zhao, Y. Robust Amphiphobic Few-Layer Black Phosphorus Nanosheet with Improved Stability. *Advanced Science* **2019**.
- Ma, P.; Wang, C.; Gao, Y.; Gu, X.; Cheng, B.; Fang, Z.; Xiong, G.; Wu, J. The Coupling Effect of Organosilicon Hydrophobic Agent and Cement on the Water Resistance of Phosphogypsum. *Materials* **2022**, *15*, 845.
- Guo, M.-Z.; Maury-Ramirez, A.; Poon, C. S. Self-cleaning ability of titanium dioxide clear paint coated architectural mortar and its potential in field application. *Journal of Cleaner Production* **2016**, *112*, 3583–3588.
- Tudu, B. K.; Kumar, A. Robust and durable superhydrophobic steel and copper meshes for separation of oil-water emulsions. *Prog. Org. Coat.* **2019**, *133*, 316.
- Thoeny, Z. A. R. The Effect of Particle Size Distribution on some Properties of Gypsum. *Key Engineering Materials* **2020**, *857*, 145. Caselle, C.; Bonetto, S.; Vagnon, F.; Costanzo, D. Dependence of macro mechanical behaviour of gypsum on micro-scale grain-size distribution. *Géotechnique Letters* **2019**, *9*, 290.
- Wansom, S.; Chintasonkro, P.; Srijampan, W. Water resistant blended cements containing flue-gas desulfurization gypsum, Portland

cement and fly ash for structural applications. *Cement and Concrete Composites* **2019**, *103*, 134.

(23) Li, J.; Cao, J.; Ren, Q.; Ding, Y.; Zhu, H.; Xiong, C.; Chen, R. Effect of nano-silica and silicone oil paraffin emulsion composite waterproofing agent on the water resistance of flue gas desulfurization gypsum. *Construction and Building Materials* **2021**, *287*, 123055.

(24) Qi, H.; Ma, B.; Tan, H.; Su, Y.; Chen, P.; Lu, W. Properties of β -HPG pastes in the presence of α -HPG prepared from phosphogypsum. *Constr. Build. Mater.* **2022**, *334*, No. 127414.

(25) Duan, Z.; Li, J.; Li, T.; Zheng, S.; Han, W.; Geng, Q.; Guo, H. Influence of crystal modifier on the preparation of α -hemihydrate gypsum from phosphogypsum. *Construction and Building Materials* **2017**, *133*, 323.

(26) Ren, T.; Xi, R.; Yang, J. Influence of autoclaved pretreatment on the properties of phosphogypsum-based composite binders. *IOP Conf. Ser.: Earth Environ. Sci.* **2017**, *81*, No. 012015.

(27) Huang, J.; Min, J.; Hu, H.; Manuka, M.; Yin, Y.; Zhou, F.; Deng, H.; Yang, R.; Tang, P.; Ma, B. Effect of mixed cation acetate electrolyte on synthesis of α -hemihydrate gypsum from phosphogypsum. *J. Am. Ceram. Soc.* **2024**, *107*, 107.

(28) Xia, B.; Shi, R.; Wang, W.; Peng, W.; Cao, Y.; Huang, Y.; Fan, G. Preparation of α -hemihydrate gypsum whiskers from phosphogypsum using atmospheric pressure nitrate solution. *Construction and Building Materials* **2024**, *412*, 134888.

(29) Ganesapillai, M.; Regupathi, I.; Murugesan, T. Characterization and Process Optimization of Microwave Drying of Plaster of Paris. *Drying Technology* **2008**, *26*, 1484.

(30) Zhang, L.; Mo, K. H.; Tan, T. H.; Hung, C.-C.; Poh, Y. S.; Ling, T.-C. Influence of calcination and GGBS addition in preparing β -hemihydrate synthetic gypsum from phosphogypsum. *Case Stud. Constr. Mater.* **2023**, *19*, No. e02259. Chen, X.; Liu, Y.; Wu, Q.; Ding, Y.; Wang, Q.; Tang, W.; Zhu, B. Study on physical and chemical characteristics of β -hemihydrate phosphogypsum. *Case Stud. Constr. Mater.* **2022**, *17*, No. e01461.

(31) Geraldo, R. H.; Costa, A. R. D.; Kanai, J.; Silva, J. S.; Souza, J. D.; Andrade, H. M. C.; Gonçalves, J. P.; Fontanini, P. S. P.; Camarini, G. Calcination parameters on phosphogypsum waste recycling. *Construction and Building Materials* **2020**, *256*, 119406.

(32) Yang, G.; Chen, Z.; Lv, C.; Deng, L.; Luo, X.; Li, Y.; He, S.; Liu, Q. Preparation and Performance of H-PDMS/PMHS/OTS Hybrid Nanosilica Hydrophobic and Self-Cleaning Coatings on Phosphogypsum Surface. *Polymers* **2023**, *15*, 3574.

(33) Zheng, T.; Miao, X.; Kong, D.; Wang, L.; Cheng, L.; Yu, K. Proportion and Performance Optimization of Lightweight Foamed Phosphogypsum Material Based on an Orthogonal Experiment. *Buildings* **2022**, *12*, 207.

(34) Anjum, A. S.; Sun, K. C.; Ali, M.; Riaz, R.; Jeong, S. H. Fabrication of coral-reef structured nano silica for self-cleaning and super-hydrophobic textile applications. *Chem. Eng. J.* **2020**, *401*, No. 125859.

(35) Playà, E.; Recio, C.; Mitchell, J. Extraction of gypsum hydration water for oxygen isotopic analysis by the guanidine hydrochloride reaction method. *Chem. Geol.* **2004**, *217* (1), 89–96. Sievert, T.; Wolter, A.; Singh, N. B. Hydration of anhydrite of gypsum ($\text{CaSO}_4\cdot\text{II}$) in a ball mill. *Cem. Concr. Res.* **2005**, *35* (4), 623–630. From Cnki

(36) Li, X.; Zhang, Q. Hydration Mechanism and Hardening Property of α -Hemihydrate Phosphogypsum. *Minerals* **2019**, *9*, 733.

(37) Silva, R. G.; Nadagouda, M. N.; Patterson, C. L.; Panguluri, S.; Luxton, T. P.; Sahle-Demessie, E.; Impellitteri, C. A. Polymorph-dependent titanium dioxide nanoparticle dissolution in acidic and alkali digestions. *Environmental Science: Nano* **2014**, *1*, 284.

(38) Zhang, Q.; Xu, P.; Pang, C.; Cui, K.; Yu, C.; Huang, L. A superhydrophobic surface with a synergistic abrasion–corrosion resistance effect prepared by femtosecond laser treatment on an FeMnSiCrNiNb shape memory alloy coating. *New J. Chem.* **2022**, *46* (40), 19188–19197.

(39) Xu, L.; Wan, J.; Yuan, X.; Pan, H.; Wang, L.; Shen, Y.; Sheng, Y. Preparation of durable superamphiphobic cotton fabrics with self-

cleaning and liquid repellency. *J. Adhes. Sci. Technol.* **2022**, *36* (1), 1–20.

(40) Yu, H.; Lian, Z.; Wan, Y.; Weng, Z.; Xu, J.; Yu, Z. Fabrication of durable superamphiphobic aluminum alloy surfaces with anisotropic sliding by HS-WEDM and solution immersion processes. *Surface & Coatings Technology* **2015**, *275*, 112–119. From Cnki

(41) Shao, C.; Jiang, M.; Zhang, J.; Zhang, Q.; Han, L.; Wu, Y. Construction of a superhydrophobic wood surface coating by layer-by-layer assembly: Self-adhesive properties of polydopamine. *Appl. Surf. Sci.* **2023**, *609*, 155259.